Large-Amplitude Oscillatory Motion of Mercury's Cross-tail Current Sheet

Gangkai Poh[1,2], Weijie Sun[3], Kellyn M. Clink[3], James A. Slavin[3], Ryan M. Dewey[3], Xianzhe Jia[3], Jim M. Raines[3], Gina A. DiBraccio[2], Jared R. Espley[2]

1 Center for Research and Exploration in Space Sciences and Technology II, University of Maryland Baltimore County, Baltimore, MD 21250, USA,

2 Solar System Exploration Division, NASA Goddard Space Flight Center, Greenbelt, Maryland, USA.

3 Department of Climate and Space Sciences and Engineering, University of Michigan, Ann Arbor, MI 48109, USA,

This is the author manuscript accepted for publication and has undergone full peer review but has not been through the copyediting, typesetting, pagination and proofreading process, which may lead to differences between this version and the Version of Record. Please cite this article as doi: 10.1029/2020JA027783

Abstract:

We surveyed four years of MESSENGER magnetic field data and analyzed intervals with observations of large-amplitude oscillatory motions of Mercury's cross-tail current sheet, or flapping waves, characterized by a decrease in magnetic field intensity and multiple reversals of B_x, oscillating with a period on the order of ~4 – 25 seconds. We performed minimum variance analysis (MVA) on each flapping wave event to determine the current sheet normal. Statistical results showed that the flapping motion of the current sheet caused it to warp and tilt in the *y*–*z* plane, which suggests that these flapping waves are kink-type waves propagating in the cross-tail direction of Mercury's magnetotail. The occurrence of flapping waves shows a strong preference in Mercury's duskside plasma sheet. We compared our results with the magnetic double-gradient instability model and examined possible flapping wave excitation mechanism theories from internal (e.g. finite gyroradius effects of planetary sodium ions Na^+ on magnetosonic waves) and external (e.g. solar wind variations and K-H waves) sources.

1. Introduction

Continuous *in-situ* magnetic field and plasma measurements observed by MESSENGER have allowed us to gain insights on the dynamic processes occurring in different regions of Mercury's magnetotail, from the northern and southern tail lobes to the cross-tail current sheet embedded within the central plasma sheet [*Slavin et al.,* 2012; *DiBraccio et al.,* 2015a; *Poh et al.,* 2017a; *Rong et al.,* 2018; *Sun et al.,* 2020]. Although the structure and processes occurring in Mercury's magnetotail are known to be qualitatively similar to that of Earth's, they are different in spatial and temporal scale [e.g. *Raines et al.,* 2011; *Gershman et al.,* 2014; *Sun et al.,* 2015; *Poh et al.,* 2017b]. Recent simulation studies [*Liu et al.,* 2019; *Chen et al.,* 2019] suggest that kinetic-scale dynamics and instabilities dominate in Mercury's small magnetotail (~10 d_i wide, where d_i is the ion inertial length), thereby explaining the observed asymmetric structure and occurrence of processes in the tail.

The oscillatory (or flapping) motion of Earth's cross-tail current sheet has been extensively studied by various missions, such as THEMIS [*Sun et al.,* 2014] and Cluster [*Zhang et al.,* 2002; *Sergeev et al.,* 2003; *Runov et al.,* 2005; *Sun et al.,* 2010; *Rong et al.,* 2015; 2018; *Gao et al.,* 2018] and is commonly identified in the magnetic field measurements as multiple reversals of the x-component of the magnetic field B_X (i.e. multiple crossings of the current sheet) [*Speiser and Ness,* 1967]. Note: the Geocentric Solar Magnetospheric (GSM) coordinate system is commonly used in these Earth studies where the *x*-axis points towards the Sun along the Sun-Earth line, the *z*-axis is the projection of the Earth's dipole axis onto the plane perpendicular to the x-axis and the *y*-axis completes the right-handed system. These statistical studies have shown that such oscillatory motion of Earth's cross-tail current sheet has an average period of ~1 – 10 minutes and generally propagate as a wave in the dawn-dusk direction from the midnight meridian to the tail flanks at

velocities of few tens of km/s. As such, the current sheet is predominantly tilted in the *y*–*z* plane during the observations of these flapping waves [*Sergeev et al.,* 2006; *Volwerk et al.,* 2013]. Earlier correlation studies further suggested a relationship between the occurrence of flapping waves at Earth and magnetic reconnection-related phenomena such as fast magnetospheric flows [e.g., *Davey et al.,* 2012] and substorm activities [*Sergeev et al.,* 2006]. Figure 1 shows an illustration of the kink-type magnetotail oscillations propagating in the dawn-dusk direction (see *Rong et al.,* [2015] for illustrations of flapping waves observed at Earth). For this type of magnetotail flapping motion, the sinusoidal flapping waves propagate in the cross-tail direction (blue dashed arrows) with the cross-tail current sheet tilted in the *y*–*z* plane (as shown by the "tilted" current sheet normal ***n***) during each crossing of the center of the current sheet at times t_1, t_2, t_3 and t_4. Therefore, the current sheet normal vectors between adjacent current sheet crossings are expected to "oscillate" in the *y*–*z* plane (i.e. change in the sign of the *y*-component with small *x*-component of the current sheet normal) as shown in Figure 1a; the spacecraft is expected to observe multiple polarity reversals of B_X for this type of magnetotail oscillation mode. Note that the time periods when the spacecraft observed the positive and negative part of the B_X reversal and their respective amplitudes are dependent on the spacecraft trajectory relative to the average location of the center of the sinusoidal current sheet in the frame of the flapping current sheet. We would like to emphasize that the use of directional terms (e.g. dawn-dusk and north-south) in this paper does not represent any specific directionality (i.e. dawn-dusk may represents dawn to dusk or dusk to dawn).

Not unique to Earth, these flapping motions of the cross-tail current sheet are also observed in other intrinsic and induced planetary magnetospheres, such as those of the giant planets (Jupiter and Saturn) [*Volwerk et al.,* 2013], Venus [*Rong et al.,* 2015], Mars [*DiBraccio et al.,* 2017], and Mercury [*Poh et al.,* 2017; 2018]. Despite the limited analysis of the flapping waves using only

single-spacecraft measurements from most planetary missions, statistical results show that the flapping waves observed in planetary magnetotails are generally similar to those observed at Earth where the flapping current sheets are also tilted in the *y*–*z* plane, consistent with the idea that the flapping waves propagate towards or away from the flanks [*Volwerk et al.,* 2013].

A natural follow-up question is: what is the formation mechanism for these current sheet oscillations? Statistical studies at Earth [e.g. *Sergeev et al.,* 2006] suggested that these dawn-dusk propagating waves are most likely to be driven by an internal source within the magnetotail. Based on spacecraft observations, several flapping wave excitation mechanisms, such as the ballooning-type [*Golochanskaya and Maltsev,* 2005] and the magnetic double-gradient instability [*Erkaev et al.,* 2007; 2008; 2009a,b; 2010; *Duan et al.,* 2018; *Korovinskiy et al.,* 2016; 2018], have been proposed. Observational studies at Earth [*Forsyth et al.,* 2009; *Sun et al.,* 2014] demonstrated that the magnetic double-gradient instability model best describes the observational data. Other observational [*Shen et al.,* 2008; *Forsyth et al.,* 2009] and numerical [*Sergeev et al.,* 2008; *Juusola et al.,* 2018] studies had also proposed solar wind variations as an external source for the excitation of flapping waves within Earth's magnetotail.

In this study, we seek to determine the differences and similarities of current sheet flapping in Mercury's magnetotail, where kinetic-scale instabilities dominate [*Liu et al.,* 2019; *Chen et al.,* 2019], and Earth's magnetotail, which is well-described by MHD. We would like to emphasize that MESSENGER is a single-spacecraft mission. Unfortunately, many of the multi-spacecraft analysis techniques employed to accurately determine the physical properties (e.g. propagation direction and speed) of these flapping waves are unavailable in our single-spacecraft Mercury study. Therefore, with MESSENGER's single-spacecraft measurements, we are restricted to the use of the minimum variance analysis (MVA) technique [*Sonnerup and Scheible,* 1998] to analyze

and infer some of the properties of the large-amplitude flapping waves observed at Mercury. The MVA technique had also been successfully applied to many earlier studies using single-point measurements at Earth (e.g. AMPTE/IRM satellite [*Sergeev et al.,* 1998] and Geotail [*Sergeev et al.,* 2006]) and other planets (e.g. Galileo and Cassini [*Volwerk et al.,* 2013]). Our statistical results show that the current sheet oscillations observed in Mercury are similar to those observed at Earth in that Mercury's current sheet during flapping motion is also tilted in the *y*–*z* plane, suggesting that the waves propagates in the cross-tail direction. We compared our results with the magnetic double-gradient instability model, and examined different internal- and external-source formation theories and models proposed previously.

2. Flapping Waves Event Selection and Data Analysis

In this study, we surveyed the full-resolution 20 vectors/second magnetic field [*Anderson et al.,* 2007] measurements from MESSENGER's magnetometer (MAG) to identify magnetotail crossings with observations of current sheet flapping wave event. We chose the aberrated Mercury Solar Magnetospheric (MSM') coordinate system for the analyses performed in this study. The Mercury Solar Magnetospheric (MSM) coordinate system is a coordinate system centered on Mercury's internal offset dipole [*Anderson et al.,* 2011] with the positive *X*-axis in the sunward direction (i.e. anti-parallel to the solar wind flow) along the Sun-Mercury line, the *Z*-axis is positive northward parallel to Mercury's magnetic dipole moment axis, and the *Y*-axis completes the right-handed system. A correction for solar wind aberration is then applied to the MSM coordinate system to create the MSM' coordinate system. This correction assumes a radial solar wind speed of 400 km/s and uses Mercury's perpendicular orbital velocity computed daily.

2.1 19th May 2012 Event

Figure 2 shows an example of MESSENGER's observation of Mercury's magnetotail on 19th May 2012. Figure 2a and 2b shows MESSENGER's trajectory through Mercury's magnetotail in the meridional (i.e. *x*–*z*) and equatorial (i.e. *x*–*y*) plane, respectively. With its polar orbital trajectory, MESSENGER traversed Mercury's dusk-side magnetotail in the *z*–direction. Figure 2c shows the magnetic field measurements observed by MESSENGER during the traversal. Panel 1 of Figure 2c shows the wavelet analysis [*Jenkins and Watts,* 1968] of the *x*–component of the observed magnetic field while Panels 2 – 5 show the x, y, z–components, and magnitude of the observed magnetic field vectors. The interval starts with MESSENGER in the southern lobe of Mercury's magnetotail characterized by the strong magnetic field predominantly in the negative B_X direction and low level of fluctuations in magnetic field. During this time period, MESSENGER observed a full (red dashed line) and several partial current sheet crossings (blue arrow). The former type of current sheet crossing is characterized by a positive-to-negative or negative-to-positive reversal of B_X, indicating that MESSENGER crosses the center of Mercury's cross-tail current sheet. The latter is characterized by a decrease in the magnitude of B_X without a reversal in the sign of B_X, indicating that MESSENGER observed the flapping motion of the current sheet but did not cross its center (i.e. $B_X = 0$ nT).

At ~14:34:30 UTC, MESSENGER entered the cross-tail current sheet proper shown by the overall "slow" reversal of B_X from negative to positive, which is due to MESSENGER traversing though Mercury's magnetotail. MESSENGER further observed frequent multiple large-amplitude B_X reversals of ~20 – 40nT, superimposed on the overall slow reversal of B_X. Wavelet analysis of the B_X oscillations (Panel 1) indicates that these flapping waves have a period of ~4 – 15s. The half-waveform of each B_X oscillations (i.e. a single flapping wave event) is identified with a red

vertical dashed line. Since MESSENGER is deep in the cross-tail current sheet, only full current sheet crossings were observed in this time interval. As MESSENGER exited the cross-tail current sheet into the northern tail lobe, MESSENGER also observed 7 partial crossing events (blue arrows) between 14:37 UTC to 14:39 UTC. Note that the partial flapping waves indicated by the blue arrows show a sharp minima and flat maxima in the absolute value of B_X. This type of waveform is consistent with the flapping current sheet scenario where the spacecraft is located north (or south) relative to the center of the flapping Harris current sheet. As the spacecraft moves away from the center of the current sheet, the gradient of B_X approaches zero, and when the spacecraft approaches the center of the current sheet, the gradient of B_X increases.

Figure 3a shows the 80-seconds-long interval between 14:35:50 UTC to 14:36:10 UTC of magnetic field measurements observed by MESSENGER in the same cross-tail current sheet encounter shown in Figure 2. Note that the time intervals with positive B_X shown in Figure 3 are systematically shorter than the time intervals with negative B_X and the absolute values of negative B_X is larger than that of positive B_X. These observed signatures are consistent with the scenario where the MESSENGER spacecraft traverses a sinusoidal current sheet (in the frame of the flapping wave) southward of the center of Mercury's cross-tail current sheet. Furthermore, the gradient of B_X peaks at $B_X = 0$ nT, which is expected during the crossing of a Harris current sheet. These observations confirm that the variation in B_X is not random but the result of a sinusoidal flapping motion of the cross-tail current sheet.

For each flapping wave event identified visually, we performed the minimum variance analysis [*Sonnerup and Scheible,* 1998] to determine the current sheet normal $\boldsymbol{n}$. Figure 3b shows the hodograms of the MVA result of a flapping wave example identified in Figure 3a at ~14:35:49 UTC (red arrow). The hodograms show a clear rotation in B_{max} with some and no variation in B_{int}

and B_{min}, respectively, signatures typically representative of a CS crossing [*Sonnerup and Scheible*, 1998]. The minimum $\boldsymbol{v}_{min}$ (i.e. current sheet normal $\boldsymbol{n}$), intermediate $\boldsymbol{v}_{int}$ and maximum $\boldsymbol{v}_{max}$ eigenvectors are [-0.01, -0.76, 0.65], [0.03, -0.65, -0.76] and [0.99, 0.03, 0.01]. We calculated the *int–min* and *max–int* eigenvalue ratios to be ~8.36 and 11.68, respectively. Using the error estimation method outlined in *Khrabrov and Sonnerup,* [1998a], we also computed the angular uncertainty $|\Delta\varphi|$ of the minimum eigenvectors for rotation towards or away from the intermediate and maximum eigenvectors (i.e. angular uncertainty cone around the current sheet normal vector) to be ~ 3.2° and 0.8°, respectively. Recent flapping wave studies [e.g. *DiBraccio et al.,* 2017] use an eigenvalue ratio threshold of 3 to establish acceptability of MVA results. The large eigenvalue ratios (i.e. greater than 3) and the small calculated angular uncertainty cone indicate that the current sheet normal for this flapping wave example is well-defined. It is interesting to note that **n** (or $\boldsymbol{v}_{min}$) is tilted in the *y–z* plane as shown by the significantly larger values of n_y and n_z as compared to n_x, which is consistent with flapping waves observed at Earth and other planets (e.g. *Volwerk et al.,* [2013] and references therein).

Table 1 shows the current sheet normal vectors with their associated angular uncertainties and eigenvalue ratios determined from MVA for all flapping waves events identified in this interval. Similar to the previous flapping wave example, the majority of the current sheet normal vectors **n** of all flapping wave events within the interval have minor component in the *x*-direction with significant components in either *y*– or *z*–direction or both, indicating that these cross-tail current sheets are tilted in the *y–z* plane. Our results also show a general pattern of most current sheet normal vectors "oscillating" in the *y–z* plane, where the *y*–component of **n** alternates in polarity between adjacent crossings. These observations are consistent with the encounter of a sinusoidal (or kink-type) flapping current sheet travelling in the cross-tail direction (e.g. *Volwerk et al.,*

[2013] and references therein). Note that it is unclear whether the flapping waves are travelling away from or towards the magnetotail flanks since we are unable to determine the actual direction of propagation with single-spacecraft measurements.

The error analysis of the MVA results also shows that the majority of the current sheet normal computed are generally reliable as reflected by the small angular uncertainty of the minimum eigenvector and/or the *int–min* eigenvalue ratios greater than 3, with the exception of few events (e.g. Event #7), which have large uncertainty angle cones due to their small *int–min* eigenvalue ratios. However, it is not surprising to observe MVA results with low *int–min* eigenvalue ratios for Mercury's cross-tail current sheet, which can be generally described by a Harris current sheet model [*Poh et al.*, 2017]. A small *int–min* eigenvalue ratio is generally expected of a Harris current sheet, which has a direction of maximum variance only [*Forsyth et al.*, 2009]. An accurate estimate of the normal using MVA technique can be obtained with sufficient measurements when there is sufficient deviation from the Harris model (i.e. presence of magnetic field component in the cross-tail direction or a magnetic shear). Therefore, only flapping wave events with *int–min* eigenvalue ratio greater than 3 will be used for subsequent statistical analysis. Despite the limitations of using the MVA technique to determine the cross-tail current sheet normal with single-spacecraft measurements, it is evident that the results from the MVA technique have captured the general behavior of the flapping motion of Mercury's cross-tail current sheet reasonably well.

2.2 Statistical Analysis

We surveyed four years of MESSENGER magnetic field data and visually identified 65 magnetotail encounters where large-amplitude, quasi-periodic magnetic field oscillations

associated with flapping motion of Mercury's cross-tail current sheet were observed. In each magnetotail encounter with large-amplitude magnetic field oscillations, the characteristic B_X reversal signatures associated with the encounter of flapping waves were visually identified to distinguish between intervals with flapping waves and random magnetic field fluctuations or electromagnetic waves [*Boardsen et al.,* 2012]. Minimum variance analysis technique was then performed on each flapping wave event to determine the vector normal to the current sheet. Every MVA results were also visually inspected to ensure that the selected events are not associated with other magnetic structures (e.g. flux ropes [*DiBraccio et al.,* 2015b] and dipolarization fronts [*Sundberg et al.,* 2012; *Sun et al.,* 2016; *Dewey et al.,* 2017, 2018]) observed in Mercury's magnetotail. A total of 638 flapping wave events were selected for further analysis.

Figure 4a and 4b show the distribution of the current sheet normal vectors in the *y*–*z* and *x*–*z* plane, respectively. Figure 4a shows that the current sheet normal vectors **n** are distributed near the unit circle in the *y*–*z* plane (i.e. $\sqrt{n_z^2 + n_y^2} = 1$), while the vectors were distributed around $n_x = 0$ in the *x*–*z* plane as shown in Figure 4b. Our result strongly indicates that $|n_x| << |n_y|, |n_z|$, which means that the current sheet associated with these flapping motions is predominantly tilted (or warped) in the *y*–*z* direction. This characteristic *y*–*z* tilt in the current sheet associated with flapping waves observed at Mercury is similar to those observed at Earth from Geotail measurements [*Sergeev et al.,* 2006], where the distribution of MVA normal in the *y*–*z* plane indicates a "*yz*–kink" type of flapping waves. Assuming that the flapping waves are planar structures, if the flapping waves were travelling in the downtail (±*x*) or cross-tail (±*y*) direction, one would expect the warping of the current sheet normal to be in the *x*–*z* or *y*–*z* plane, respectively. Hence, within the limits of single-spacecraft measurements, our results suggest that these flapping waves are

likely to be travelling in the cross-tail direction with the orientation of the current sheet normal similar to that observed at Earth [*Sergeev et al.,* 2006] and the giant planets [*Volwerk et al.,* 2013].

We calculated the typical periods of the flapping waves from the results of the wavelet analysis. Figure 4c shows the distribution of flapping wave periods of all identified peaks in wave power associated with groups of flapping wave events. The distribution in Figure 4c shows a large range of flapping wave period of ~4 – 25s and the average flapping wave period (oscillation frequency) is ~12s (0.52 rad/s), which is much smaller than that observed at Earth and the outer planets (~2 – 10 minutes [*Kubyshkina et al.,* 2014; *Volwerk et al.,* 2013]). Such significant difference in flapping period can be attributed to Mercury's smaller scale and more dynamic magnetosphere, and extreme solar wind conditions in the inner heliosphere [e.g. *Slavin et al.,* 2014; 2019; *Jia et al.,* 2019]

We also examined whether there is any dawn-dusk asymmetry in the occurrence of flapping waves at Mercury. Figure 5a shows the distribution of flapping wave occurrences as a function of Y_{MSM}. Interestingly, there is a strong duskward preference of the flapping wave events identified in this study in Mercury's cross-tail current sheet with peak occurrence at $Y_{MSM} \sim 1R_E$. Note that this observed strong asymmetry is unlikely due to orbital selection bias during the survey of MESSENGER data as the spacecraft orbital trajectory precesses around Mercury's rotation axis, resulting in even local time coverage over one full precession. This dawn-dusk asymmetry in the occurrence of current sheet flapping waves is unique to Mercury since such asymmetry has not been observed in other planets. Possible relationships between the known asymmetries of Mercury's magnetotail and the observed duskward preference of flapping wave occurrence, and its implication on the excitation mechanism of Mercury's current sheet flapping waves will be further examined in the Discussion section.

3. Discussion

Our analysis of Mercury's flapping waves shows that Mercury's cross-tail current sheet oscillates with periods of ~4 – 25s, and that this flapping motion of the current sheet caused it to warp and become tilted in the *y*-*z* plane. This tilted current sheet geometry is similar to that of the flapping waves observed at Earth and is consistent with the scenario where the flapping waves are propagating in the cross-tail direction. Since we cannot accurately determine the actual flapping wave propagation direction using single-spacecraft measurements, it is possible that these oscillatory motions of Mercury's current sheet are driven by an internal process within the magnetotail and/or external solar wind-driven processes. The natural follow-up question would be: what is the most plausible internal and/or external formation process or mechanism for Mercury's flapping waves?

3.1 Ballooning-type Flapping Wave Model

Multiple models had been proposed to explain the formation and observations of flapping waves via an internal process at Earth. The ballooning-type [*Golovchanskaya and Maltsev*, 2005] and magnetic double-gradient instability models [*Erkaev et al.,* 2007] are widely-accepted internal flapping wave formation models. The Ballooning-type model, similar to the interchange instability with magnetic tension on curved field lines serving the same role as gravitational force, requires the scale of the wavelength to be much smaller than the radius of curvature of the field lines (R_C) [*Pritchett and Coroniti,* 2010]. In the midtail region (i.e. $-1.8\ R_M > X_{MSM} > -3.8\ R_M$) of Mercury's duskside current sheet where most flapping waves were observed, R_C ~200 km [*Rong et al.,* 2018]. We further assumed the characteristic wavelength of these flapping waves to be on the order of or larger than Mercury's cross-tail current sheet thickness (~0.4 R_M or ~976 km [*Poh et al.,* 2017a]). This is a valid assumption since the typical wavelength of flapping waves observed at Earth is

several R_E [*Sergeev et al.*, 2003; *Runov et al.*, 2005; *Wang et al.*, 2019], which is an order of magnitude larger than the average terrestrial cross-tail current sheet thickness during substorm conditions (~0.1 R_E [*Sergeev et al.*, 1990]). Since the wavelength of the flapping waves is much larger than R_C of Mercury's duskside cross-tail current sheet, it is unlikely that the flapping waves observed at Mercury are caused by the ballooning-type instability.

3.2 Magnetic Double-Gradient Instability Flapping Wave Model

The magnetic double-gradient instability can occur when there is a "tailward B_Z gradient" magnetic field topology in the cross-tail current sheet, resulting in the unstable perturbation of the current sheet due to the force imbalance between the magnetic stress and total pressure gradient force in the quiescent current sheet along the *z*–direction (see Figure 4 in *Erkaev et al.*, [2008] for illustration). This perturbation of the current sheet drives the flapping waves in the cross-tail direction. Although both kink and sausage mode waves can be excited by this instability, *Erkaev et al.*, [2008] demonstrated that the kink mode waves are more likely to be observed since it has a faster growth rate than the sausage mode. The characteristic oscillation frequency ω_f of the current sheet [*Erkaev et al.*, 2008, 2010; *Forsyth et al.*, 2009], depends on the product of the spatial gradients of B_X and B_Z, and is given by the equation:

$$\omega_f = \sqrt{\frac{1}{\mu_0 m_p n_0}\left\langle\frac{\partial B_X}{\partial z}\right\rangle\frac{\partial B_Z}{\partial x}}\Bigg|_{z=z_0} \quad (1)$$

where n_0 is the plasma density, $\frac{\partial B_X}{\partial z}$ and $\frac{\partial B_Z}{\partial x}$ are the spatial gradients of B_X and B_Z at the center of the cross-tail current sheet ($z = z_0$), respectively.

This "tailward B_Z gradient" (or $\frac{\partial B_Z}{\partial x} < 0$) magnetic field topology can be caused by the local thinning of the cross-tail current sheet in the near-tail region [*Erkaev et al.*, 2008]. The follow-up question

is: how strong should the tailward B_Z gradient, if it exists, be for the double-gradient instability to create the observed quasi-periods of Mercury's flapping waves?

As a first order approximation, we calculated $\left.\frac{\partial B_X}{\partial z}\right|_{z=z_0}$ ~165 nT-(R_M)$^{-1}$ by differentiating the Harris current sheet equation at $z = z_0$, with the asymptotic lobe field B_0 and duskside current sheet half-thickness Δ to be ~41.4 nT and 0.25 R_M, respectively [*Poh et al.*, 2017a]. Assuming n_0 ~1 cm^{-3} for Mercury's central plasma sheet [*Raines et al.*, 2013; *Gershman et al.*, 2014; *Poh et al.*, 2018]) and $<\omega_f>$ ~0.52 rad/s determined from the wavelet analysis, we calculated the value of $\left.\frac{\partial B_Z}{\partial x}\right|_{z=z_0}$ required to create the observed current sheet oscillations to be ~19.52 nT/R_M (~0.008 nT/km). Taking into consideration Hall effects in the double-gradient instability model [*Erkaev et al.*, 2010], we further calculated the characteristic oscillation speed V_f (i.e. $\omega_f\Delta$) to be ~317 km/s and the dimensionless Hall parameter α (i.e. ratio of proton current speed to the characteristic oscillation speed) to be ~0.4 [*Erkaev et al.*, 2010]. We then determined the flapping wave group velocity V_g to be ~0.5V_f = 158 km/s using the Hall parameter α of 0.4 solid curve in Figure 2a of *Erkaev et al.*, [2010]. It is worth noting that the calculated propagating velocity of Mercury's flapping waves is closer to the upper limit of the flapping waves observed at Earth, which ranges from few tens [*Runov et al.*, 2005; *Sun et al.*, 2014] to hundreds of km/s [*Sergeev et al.*, 2006].

Our calculated gradient is approximately two orders of magnitude larger than that of Earth's (~6x10^{-5} nT/km) [*Erkaev et al.*, 2007], raising the question of whether such tailward B_Z gradient configuration is possible in Mercury's magnetotail. Simulations [*Hsieh and Otto*, 2015] and observation [*Sun et al.*, 2017a] at Earth have shown that magnetic flux depletion may occur in the Earth's near-tail region due to the azimuthal transport of closed magnetic flux from nightside to dayside along contours of constant flux tube entropy, resulting in current sheet thinning in the

near-tail region. This process could make the B_Z gradients in the cross-tail current sheet necessary to drive these kink-type current sheet oscillations at Mercury and should be further investigated in future simulation and observation studies.

3.3 External Excitation Mechanisms of Flapping Waves

The excitation of current sheet flapping waves inside planetary magnetotails due to solar wind variations as an external driving mechanisms has also been explored from observational and modelling perspectives. Solar wind pressure perturbation initiated motion of the cross-tail current sheet has been observed by *McComas et al.* [1986], *Shen et al.,* [2008], and more recently, *Wang et al.* [2019]. The numerical model by *Sergeev et al.,* [2008] showed that the total pressure difference between the north and south tail lobe caused by a solar wind directional discontinuity can result in vertical motion of the neutral sheet initiated at the tail center. *Juusola et al.,* [2018] further demonstrated in their hybrid-Vlasov model that a north-south asymmetric magnetopause perturbation can displace the initial current and launch a standing magnetosonic wave within the tail resonance cavity. Both models suggest that the displacement of the neutral sheet by solar wind drivers can excite kink-like waves propagating from the tail center towards the flanks. Earlier Mercury studies on reconnection dynamics [e.g. *DiBraccio et al.,* 2013; *Slavin et al.,* 2014] show that the extreme low-β, high-dynamic-pressure solar wind conditions at Mercury drive intense reconnection and flux transfer generation at Mercury's magnetopause and, consequently, in the magnetotail. It is plausible that external solar wind drivers play an important role in exciting flapping waves within Mercury's magnetotail. However, in the absence of an upstream solar wind monitor, the question of the relationship between flapping waves' occurrence and solar wind perturbations as an external driving source can only be resolved through theory and numerical modelling.

3.4 Dawn-Dusk Asymmetric Distribution of Flapping Waves

Our statistical results also show that flapping waves are predominantly observed in Mercury's duskside cross-tail current sheet with peak occurrence at $Y_{MSM} \sim 1\ R_M$. At Earth, the peak occurrence of flapping waves were observed near the tail center [*Sergeev et al.,* 2006], which suggests that the source of flapping waves at Earth is located near the tail center. Following similar arguments to those used at Earth, this distinct preferred occurrence of Mercury's flapping waves observed at $Y_{MSM} \sim 1\ R_M$ implies a duskward shift in the internal source of flapping waves as compared to Earth. Recent studies have revealed many asymmetries in Mercury's cross-tail current sheet properties [*Poh et al.,* 2017b] and occurrence of reconnection-related phenomena. In particular, there is a dawnward preference in the occurrence of dipolarization fronts, often associated with high speed flows, in Mercury's cross-tail current sheet [*Sun et al.,* 2016; 2017b; *Dewey et al.,* 2018] as shown in Figure 5b. At Earth, studies [*Erkaev et al.,* 2009a,b] have suggested a relationship between the occurrence of bursty bulk flows (BBFs) and flapping waves, where a fast moving flow burst from a reconnection region could excite kink-like perturbations in the current sheet away from the source. However, similar processes is not applicable to Mercury since both the occurrence of dipolarization fronts and flapping waves have opposite asymmetry. On the other hand, earlier studies [*Sundberg et al.,* 2012; *Liljeblad et al.,* 2015] have shown a duskward preference in the occurrence of Kelvin-Helmholtz (K-H) waves at Mercury's magnetopause, which is similar to that of the flapping waves'. This similarity in asymmetric occurrence indicates that K-H waves could be another possible external source mechanism in exciting flapping motions of Mercury's cross-tail current sheet. To date, there have not been any studies exploring the relationship between current sheet flapping waves and the occurrence of K-H waves as an external flapping source.

Interestingly, the observed dawn-dusk asymmetric distribution of current sheet flapping wave occurrence in Mercury's cross-tail current sheet is also similar to the spatial distribution of sodium ion (Na^+) density as shown in Figure 5a and 5c. Previous MESSENGER studies using the Fast Imaging Plasma Spectrometer (FIPS) instrument [*Raines et al.,* 2013; *Gershman et al.,* 2014] reported higher observed Na^+ density in the pre-midnight (or duskside) region of Mercury's plasma sheet and this dawn-dusk Na^+ density asymmetry has also been observed in simulations [e.g. *Yagi et al.,* 2017; *Chen et al.,* 2019]. Such dawn-dusk asymmetry in Na^+ density have been associated with the Na^+ dynamics in Mercury's magnetosphere, such as escape of Na^+ from a high-energy partial sodium ring during high solar wind dynamic pressure condition [*Yagi et al.,* 2010; 2017] or centrifugal acceleration and transport of cold Na^+ from Mercury's cusp into the duskside plasma sheet via non-adiabatic Speiser-type orbits [*Delcourt* 2013]. It is possible that ion-ion hybrid resonance instability in a multi-species plasma sheet (i.e. proton and Na^+) [e.g. *Buchsbaum,* 1960] can drive fast magnetosonic waves propagating perpendicular to the magnetic field from the magnetopause towards the center of the cross-tail current sheet. These magnetosonic waves can then create localized spatial gradients in the magnetic field near the current sheet at scale lengths on the order of the Na^+ gyroradius, making the duskside cross-tail current sheet unstable to double-gradient instability. Although the flapping wave excitation mechanism described above is just as speculative as the other processes discussed in this study, it adequately explained the dawn-dusk asymmetry of the current sheet flapping wave occurrences.

From the above discussion, the excitation mechanism and duskward preference of flapping waves' occurrence at Mercury remains an open question. Future simulations (e.g. multi-fluid magnetohydrodynamics (MHD) and/or MHD embedded Particle-in-Cell models) and theoretical studies should be conducted to further explore each possibilities examined in this study to better

our understanding of the excitation mechanism of flapping waves at Mercury and its unique observed dawn-dusk asymmetry.

4. Conclusion

In summary, we analyzed 638 flapping wave events identified from 65 MESSENGER crossings of Mercury's magnetotail. Our results can be summarized as follows:

I. Frequent large-amplitude oscillations of Mercury's cross-tail current sheet characterized by multiple B_X reversals with an average period of ~12 seconds were observed.

II. We determined that the flapping motion of Mercury's cross-tail current sheet warped and tilted the current sheet in the y–z plane.

III. The flapping waves preferentially occur on Mercury's duskside current sheet, which is similar to the dawn-dusk asymmetry pattern of the Na^+ density in Mercury's plasma sheet and K-H waves on Mercury's magnetopause.

IV. The magnetic double-gradient instability is a plausible excitation mechanism for flapping wave formation at Mercury. However, other external (e.g. solar wind variations and K-H waves) and internal (e.g. finite gyroradius effects of planetary Na^+ on magnetosonic waves) processes are also possible excitation mechanisms for flapping wave formation at Mercury.

Acknowledgement

Data sets analyzed in this study are archived with the NASA Planetary Data System (PDS) (https://pds-ppi.igpp.ucla.edu/mission/MESSENGER). The MAG CDR files in the PDS were used in this study. The authors acknowledged support provided by NASA Discovery Data Analysis Program (DDAP) grants NNX15K88G, NNX15AL01G and NNX16AJ05G, Heliophysics Supporting Research (HSR) NNX15AJ68G, Living with a Star NNX16AJ67G, and Solar System Workings (SSW) Program grant NNX15AH28G to the University of Michigan. The authors thank Dr. Martin Volwerk and the anonymous second reviewer for their helpful suggestions and reviews of this manuscript.

445

446 **Figures:**

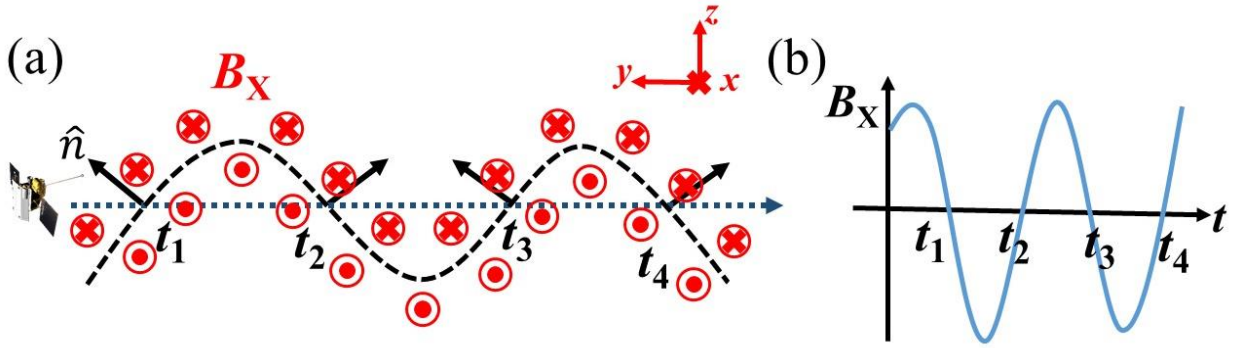

447

448 Figure 1: Illustration of kink-type flapping motion of the cross-tail current sheet. The black arrows
449 represents the current sheet normal vector while the blue dashed arrows represents the direction of
450 the current sheet motion. (b) Expected magnetic field signatures in the MSM *x*–component for
451 kink-type current sheet flapping.

452

453

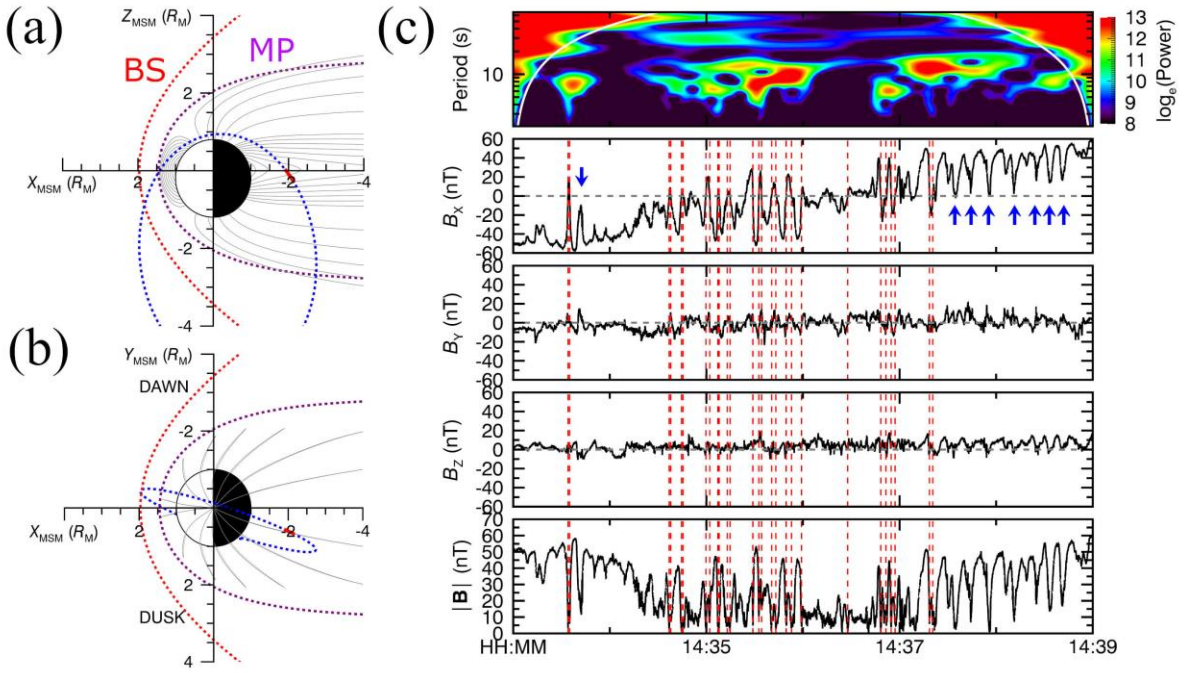

Figure 2: Orbit of MESSENGER on 19th May 2012 in the (a) meridional and (b) equatorial plane. Red and purple dashed lines represents the location of Mercury's model bow shock and magnetopause, respectively [*Winslow et al.*, 2013]. Blue dashed line represents MESSENGER's orbit around Mercury on 19th May 2012, and the gray lines shows the scaled T96 model magnetic field lines [*Tsyganenko*, 1995] using a linear scaling factor of 8. (c) Full-resolution magnetic field measurements of MESSENGER encounter of Mercury's cross-tail current sheet on 19th May 2012. Panel 1 shows wavelet analysis of B_X and Panel 2 – 5 show three components and magnitude of magnetic field measurements, respectively. Dotted red lines and blue arrows represent full and partial flapping wave events, respectively.

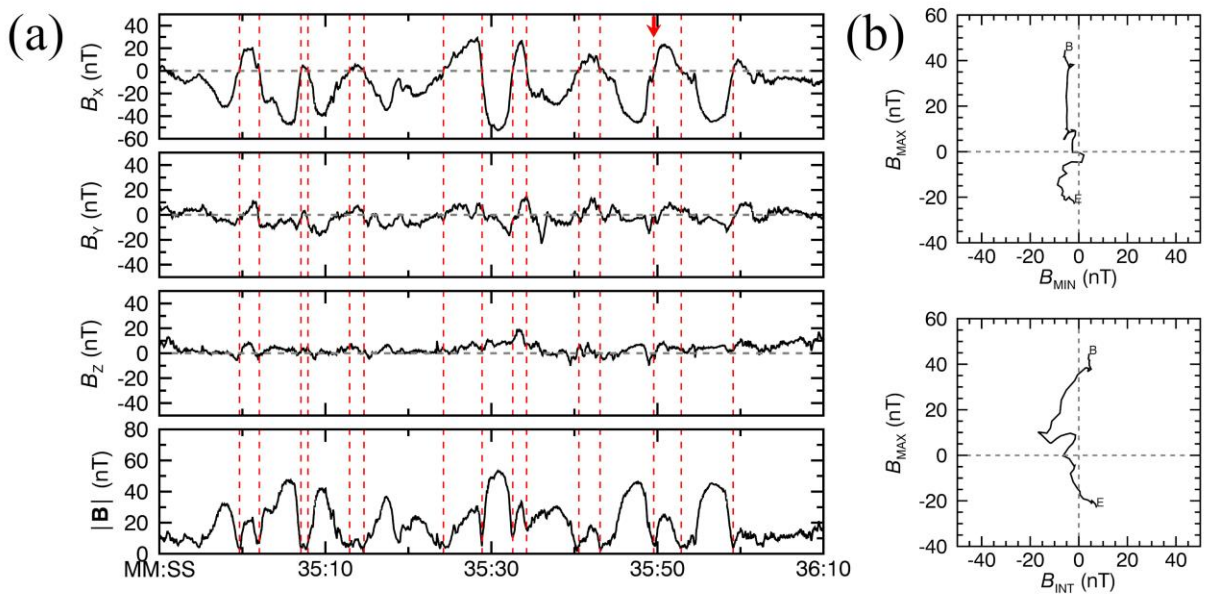

Figure 3: (a) Close-up interval of magnetic field measurements during encounter of Mercury's cross-tail current sheet observed by MESSENGER on 19th May 2012 as shown in Figure 2. (b) MVA hodogram of a flapping wave example denoted by red arrow in Figure 3(a).

	UTC (HH:MM:SS)	$\hat{\mathbf{n}}$	$\lambda_{int}/\lambda_{min}$	$\lambda_{max}/\lambda_{int}$	$\Delta\varphi_{int,min}$ (°)	$\Delta\varphi_{max,min}$ (°)
1	14:34:59	[0.07, –0.89, 0.44]	6.05	28.80	4.4	0.7
2	14:35:02	[–0.002, 0.57, 0.82]	4.53	28.40	10.9	1.6
3	14:35:07	[0.07, –0.45, 0.89]	8.27	49.88	5.1	0.6
4	14:35:08	[–0.16, 0.006, 0.99]	4.29	16.82	6.1	1.2
5	14:35:13	[–0.27, 0.43, 0.86]	2.52	47.21	7.0	0.6
6	14:35:14	[0.11, –0.09, 0.99]	2.64	13.47	7.0	1.2
7	14:35:24	[–0.17, 0.50, 0.85]	1.21	40.22	32.3	0.9
8	14:35:28	[–0.11, 0.73, 0.67]	1.97	139.42	17.3	0.7
9	14:35:32	[–0.004, –0.51, 0.86]	2.22	81.50	11.8	0.7
10	14:35:34	[–0.22, 0.15, 0.96]	3.20	23.67	9.3	1.3
11	14:35:40	[–0.28, 0.96, 0.03]	2.43	14.30	7.3	1.2
12	14:35:43	[0.03, –0.19, 0.98]	5.91	5.38	3.8	1.4
13	14:35:49	[0.01, –0.76, 0.65]	8.36	11.68	3.2	0.8
14	14:35:53	[–0.003, 0.09, 0.99]	2.23	67.26	6.9	0.5
15	14:35:59	[0.18, –0.70, 0.69]	14.13	46.26	3.0	0.4

Table 1: MVA results for flapping wave events shown in Figure 2. (*Column 3*) Current sheet normal ***n*** computed from the MVA technique. (*Column 4 – 5*) The intermediate-to-minimum and maximum-to-intermediate eigenvalues ratios. (*Column 6 – 7*) The angular uncertainties of the minimum eigenvector for rotation towards or away from the intermediate and maximum eigenvectors (i.e. angular uncertainty cone around the current sheet normal vector), respectively.

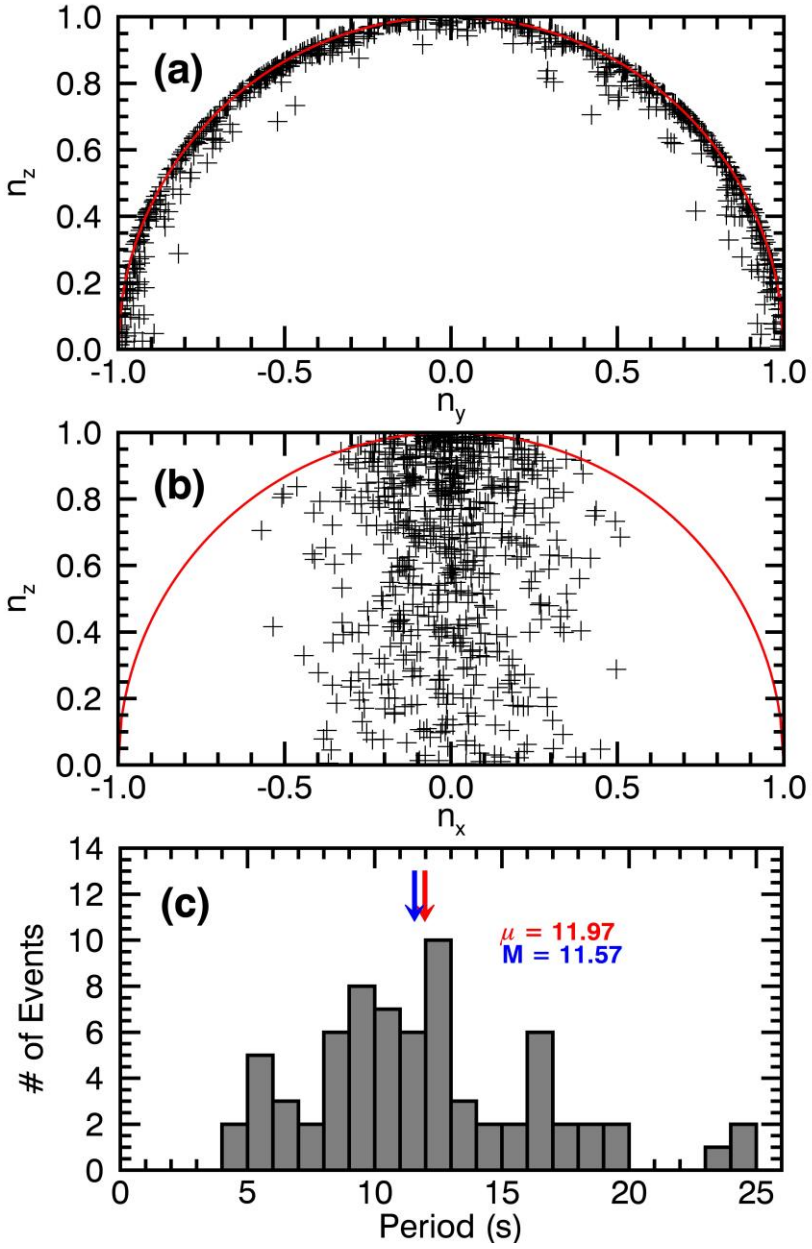

Figure 4: Distribution of current sheet normal vectors in (a) *y*–*z*, and (b) *x*–*z* plane. The red line represents the $\sqrt{n_z^2 + n_y^2} = 1$ and $\sqrt{n_z^2 + n_x^2} = 1$ curves, respectively. (c) Distribution of the periods of flapping waves. μ and M in Figure 4c represent the mean and median of the flapping wave periods respectively.

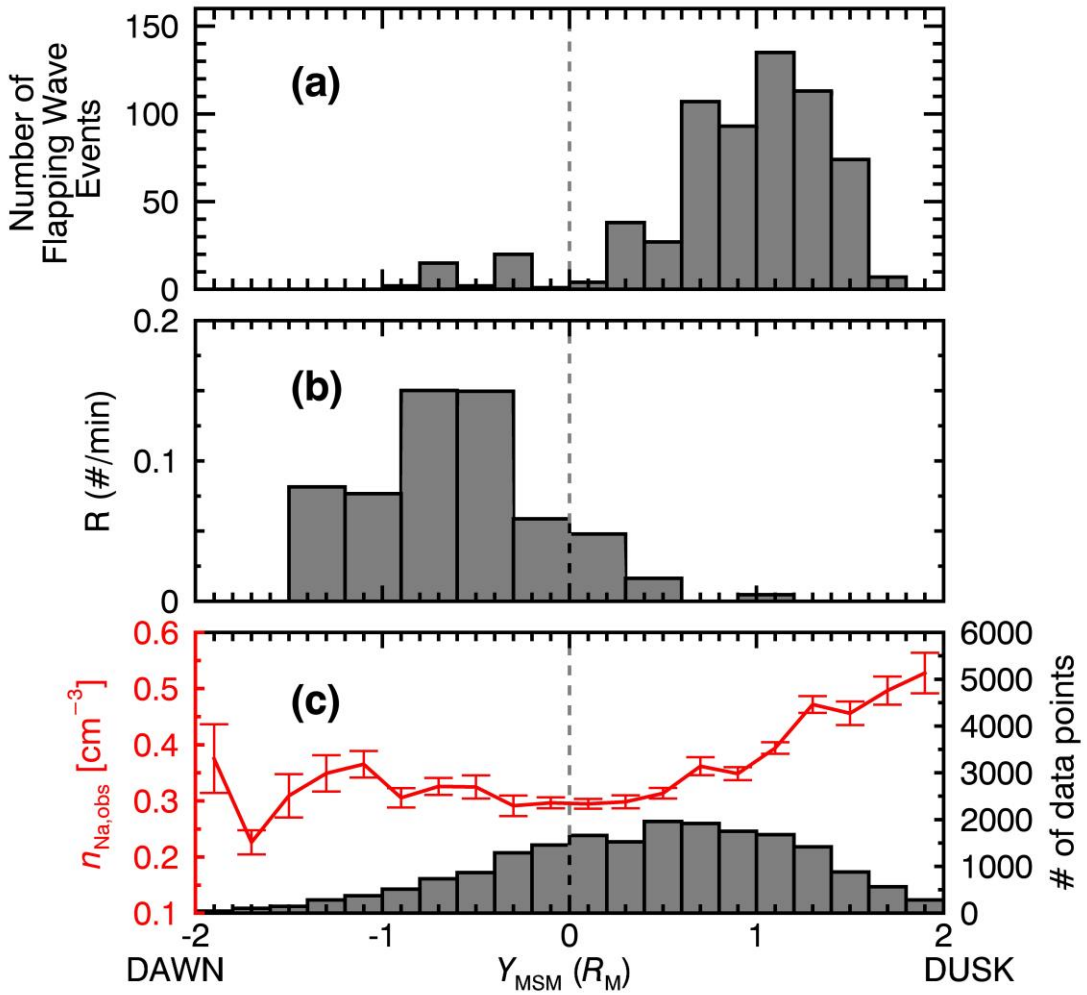

Figure 5: Dawn-dusk distribution of (a) flapping wave occurrences (bin size of 0.1 R_M), (b) occurrence rate of dipolarization fronts (bin size of 0.3 R_M) observed by MESSENGER [*Sun et al.*, 2016], and (c) observed Na^+ density (bin size of 0.1 R_M) in the cross-tail current sheet (i.e. –1.5 > X_{MSM} (R_M) > –3.5 and 0.4 > Z_{MSM} (R_M) > –0.4). The dashed line represents the noon-midnight meridian (i.e. Y_{MSM} = 0). The error bars and histogram in Figure 5c represents the standard error of the mean of the observed Na^+ density in each bin and the total number of data points in each bin, respectively.

References

Anderson, B. J., M. H. Acuña, D. A. Lohr, J. Scheifele, A. Raval, H. Korth, and J. A. Slavin (2007), The Magnetometer instrument on MESSENGER, *Space Sci. Rev., 131*, 417–450, doi:10.1007/s11214-007-9246-7.

Anderson, B. J., C. L. Johnson, H. Korth, M. E. Purucker, R. M. Winslow, J. A. Slavin, S. C. Solomon, R. L. McNutt Jr., J. M. Raines, and T. H. Zurbuchen (2011), The global magnetic field of Mercury from MESSENGER orbital observations, *Science, 333*, 1859–1862, doi:10.1126/science.1211001.

Buchsbaum, S. J. (1960). Resonance in a plasma with two ion species. *The Physics of Fluids*, *3*(3), 418-420.

Boardsen, S. A., J. A. Slavin, B. J. Anderson,H. Korth, D. Schriver, and S. C. Solomon (2012), Survey of coherent 1 Hz waves in Mercury's inner magnetosphere from MESSENGER observations, J. Geophys. Res., 117, A00M05, doi:10.1029/2012JA017822.

Chen, Y., Tóth, G., Jia, X., Slavin, J. A., Sun, W., Markidis, S., et al (2019). Studying dawn-dusk asymmetries of Mercury's magnetotail using MHD-EPIC simulations. *Journal of Geophysical Research: Space Physics*, 124. https://doi.org/10.1029/2019JA026840

Collier, M. R., and R. P. Lepping (1996), Jovian magnetopause breathing, Planet. Space Sci., 44, 187–197.

Daughton, W. (1998), Kinetic theory of the drift kink instability in a current sheet, *J. Geophys. Res.*, 103(A12), 29429– 29443, doi:10.1029/1998JA900028.

Davey, E. A., Lester, M., Milan, S. E., and Fear, R. C. (2012), Storm and substorm effects on magnetotail current sheet motion, *J. Geophys. Res.*, 117, A02202, doi:10.1029/2011JA017112.

Delcourt, D. C., Grimald, S., Leblanc, F., Berthelier, J.-J., Millilo, A., Mura, A., … Moore, E. E. (2003). A quantitative model of the planetary Na+ contribution to Mercury's magnetosphere. *Annales de Geophysique*, **21**(8), 1723–1736. https://doi.org/10.5194/angeo-21-1723-2003

Dewey, R. M., Slavin, J. A., Raines, J. M., Baker, D. N., & Lawrence, D. J. (2017). Energetic electron acceleration and injection during dipolarization events in Mercury's magnetotail. Journal of Geophysical Research: Space Physics, 122, 12,170– 12,188. https://doi.org/10.1002/2017JA024617

Dewey, R. M., Raines, J. M., Sun, W., Slavin, J. A., & Poh, G. (2018). MESSENGER observations of fast plasma flows in Mercury's magnetotail. *Geophysical Research Letters*, 45, 10,110– 10,118. https://doi.org/10.1029/2018GL079056

DiBraccio, G. A., J. A. Slavin, J. M. Raines, D. J. Gershman, P. J. Tracy, S. A. Boardsen, T. H. Zurbuchen, B. J. Anderson, H. Korth, R. L. Jr. McNutt, et al. (2015a), First observations of Mercury's plasma mantle by MESSENGER, *Geophys. Res. Lett.*, 42, 9666–9675, doi: 10.1002/2015GL065805.

DiBraccio, G. A., et al. (2015b), MESSENGER observations of flux ropes in Mercury's magnetotail, Planet. Space Sci., 115, 77–89, doi:10.1016/j.pss.2014.12.016.

DiBraccio, G. A., et al. (2017), MAVEN observations of tail current sheet flapping at Mars, *J. Geophys. Res. Space Physics*, 122, 4308– 4324, doi:10.1002/2016JA023488.

Duan, A., Zhang, H., & Lu, H. (2018). 3D MHD simulation of the double-gradient instability of the magnetotail current sheet. *Science China Technological Sciences*, *61*(9), 1364-1371

Erkaev, N. V., V. S. Semenov, and Biernat H. K. (2007), Magnetic double gradient instability and flapping waves in a current sheet, Phys. Rev. Lett., 99, 235003, doi: 10.1103/PhysRevLett.99.235003.

Erkaev, N. V., V. S. Semenov, and H. K. Biernat (2008), Magnetic double gradient mechanism for flapping oscillations of a current sheet, Geophys. Res. Lett., 35, L02111, doi: 10.1029/2007GL032277.

Erkaev, N. V., V. S. Semenov, I. V. Kubyshkin, M. V. Kubyshkina, and H. K. Biernat (2009a), MHD aspect of current sheet oscillations related to magnetic field gradient, Ann. Geophys., 27, 417–425, doi:10.5194/angeo-27-417-2009.

Erkaev, N. V., V. S. Semenov, I. V. Kubyshkin, M. V. Kubyshkina, and H. K. Biernat (2009b), MHD model of the flapping motions in the magnetotail current sheet, J. Geophys. Res., 114, A03206, doi:10.1029/2008JA013728.

Erkaev, N. V., V. S. Semenov, and H. K. Biernat (2010), Hall magnetohydrodynamic effects for current sheet flapping oscillations related to the magnetic double gradient mechanism, Phys. Plasmas, 17, 060703, doi:10.1063/1.3439687.

Forsyth, C., Lester, M., Fear, R. C., Lucek, E., Dandouras, I., Fazakerley, A. N., et al. (2009). Solar wind and substorm excitation of the wavy current sheet. Annales de Geophysique, 27(6), 2457–2474. https://doi.org/10.5194/angeo-27-2457-2009

Gao, J. W., Rong, Z. J., Cai, Y. H., Lui, A. T. Y., Petrukovich, A. A., Shen, C., et al. (2018). The distribution of two flapping types of magnetotail current sheet: Implication for the flapping mechanism. Journal of Geophysical Research: Space Physics, 123, 7413– 7423. https://doi.org/10.1029/2018JA025695

Gershman, D. J., J. A. Slavin, J. M. Raines, T. H. Zurbuchen, B. J. Anderson, H. Korth, D. N. Baker, and S. C. Solomon (2014), Ion kinetic properties in Mercury's pre-midnight plasma sheet, *Geophys. Res. Lett.*, 41, 5740–5747, doi:10.1002/2014GL060468.

Golovchanskaya, I. V., and Maltsev, Y. P. (2005), On the identification of plasma sheet flapping waves observed by Cluster, *Geophys. Res. Lett.*, 32, L02102, doi:10.1029/2004GL021552.

Korovinskiy, D. B., Ivanov, I. B., Semenov, V. S., Erkaev, N. V., & Kiehas, S. A. (2016). Numerical linearized MHD model of flapping oscillations. *Physics of Plasmas*, *23*(6), 062905.

Korovinskiy, D. B., Erkaev, N. V., Semenov, V. S., Ivanov, I. B., Kiehas, S. A., & Ryzhkov, I. I. (2018). On the influence of the local maxima of total pressure on the current sheet stability to the kink-like (flapping) mode. *Physics of Plasmas*, *25*(2), 022904.

Kubyshkina, D. I., Sormakov, D. A., Sergeev, V. A., Semenov, V. S., Erkaev, N. V., Kubyshkin, I. V.,Ganushkina, N. Y., and Dubyagin, S. V. (2014), How to distinguish between kink and sausage modes in flapping oscillations?, J. Geophys. Res. Space Physics, 119, 3002– 3015, doi:10.1002/2013JA019477.

Liljeblad, E., Sundberg, T., Karlsson, T., and Kullen, A. (2015), Statistical investigation of Kelvin-Helmholtz waves at the magnetopause of Mercury, *J. Geophys. Res. Space Physics*, 119, pages 9670– 9683. doi:10.1002/2014JA020614.

Liu, Y.-H., Li, T. C., Hesse, M., Sun, W.-J., Liu, J., Burch, J., et al. (2019). Three-dimensional magnetic reconnection with a spatially confined X-line extent: Implications for dipolarizing flux bundles and the dawn-dusk asymmetry. *Journal of Geophysical Research: Space Physics*, 124, 2819– 2830. https://doi.org/10.1029/2019JA026539

Jenkins, G. M., and D. G. Watts (1968), *Spectral Analysis and its Applications*, 525 pp., Holden-Day, Boca Raton, Fla.

Juusola, L., Pfau-Kempf, Y., Ganse, U., Battarbee, M., Brito, T., Grandin, M., Turc, L., & Palmroth, M. (2018). A possible source mechanism for magnetotail current sheet flapping. Annales de Geophysique, 36(4), 1027–1035. https://doi.org/10.5194/angeo-36-1027-2018

Jia, X., Slavin, J. A., Poh, G., DiBraccio, G. A., Toth, G., Chen, Y., et al. (2019). MESSENGER observations and global simulations of highly compressed magnetosphere events at Mercury. *Journal of Geophysical Research: Space Physics*, 124, 229– 247. https://doi.org/10.1029/2018JA026166

McComas, D. J., Russell, C. T., Elphic, R. C., and Bame, S. J. (1986), The near-Earth cross-tail current sheet: Detailed ISEE 1 and 2 case studies, *J. Geophys. Res.*, 91(A4), 4287– 4301, doi:10.1029/JA091iA04p04287.

Poh, G., J. A. Slavin, X. Jia, J. M. Raines, S. M. Imber, W.-J. Sun, D. J. Gershman, G. A. DiBraccio, K. J. Genestreti, and A. W. Smith (2017a), Mercury's cross-tail current sheet: Structure, X-line location and stress balance, *Geophys. Res. Lett.*, 44, 678–686, doi: 10.1002/2016GL071612.

Poh, G., J. A. Slavin, X. Jia, J. M. Raines, S. M. Imber, W.-J. Sun, D. J. Gershman, G. A. DiBraccio, K. J. Genestreti, and A. W. Smith (2017b), Coupling between Mercury and its nightside magnetosphere: Cross-tail current sheet asymmetry and substorm current wedge formation, *J. Geophys. Res. Space Physics*, 122, 8419–8433, doi: 10.1002/2017JA024266.

Poh, G., Slavin, J. A., Jia, X., Sun, W.-J., Raines, J. M., Imber, S. M., et al. (2018). Transport of mass and energy in Mercury's plasma sheet. Geophysical Research Letters, 45, 12,163– 12,170. https://doi.org/10.1029/2018GL080601

Pritchett, P. L., and Coroniti, F. V. (2010), A kinetic ballooning/interchange instability in the magnetotail, J. Geophys. Res., 115, A06301, doi:10.1029/2009JA014752.

Raines, J. M., J. A. Slavin, T. H. Zurbuchen, G. Gloeckler, B. J. Anderson, D. N. Baker, H. Korth, S. M. Krimigis, and R. L. McNutt Jr. (2011), MESSENGER Observations of the plasma environment near Mercury, *Planet. Space Sci.*, 59, 2004–2015, doi:10.1016/pss.2011.02.004.

Raines, J. M., et al. (2012), Distribution and compositional variations of plasma ions in Mercury's space environment: The first three Mercury years of MESSENGER observations, *J. Geophys. Res. Space Physics*, 118, 1604– 1619, doi:10.1029/2012JA018073.

Rong, Z. J., Barabash, S., Stenberg, G., Futaana, Y., Zhang, T. L., Wan, W. X., Wei, Y., andWang, X.-D. (2015), Technique for diagnosing the flapping motion of magnetotail current sheets based on single-point magnetic field analysis. *J. Geophys. Res. Space Physics*, 120, 3462– 3474. doi: 10.1002/2014JA020973.

Rong Z. J., Ding Y., Slavin J. A., Zhong J., Poh G., Sun W. J., Wei Y., Chai L. H., Wan W. X. and Shen C., (2018) The Magnetic Field Structure of Mercury's Magnetotail, *Journal of Geophysical Research: Space Physics*, **123**, 1, (548-566).

Runov, A., Sergeev, V. A., Baumjohann, W., Nakamura, R., Apatenkov, S., Asano, Y., ... & Balogh, A. (2005) Electric current and magnetic field geometry in flapping magnetotail current sheets, *Annales Geophysicae*, Vol. 23, No. 4, pp. 1391-1403.

Sergeev, V., Angelopoulos, V., Carlson, C., and Sutcliffe, P. (1998), Current sheet measurements within a flapping plasma sheet, *J. Geophys. Res.*, 103(A5), 9177– 9187, doi:10.1029/97JA02093.

Sergeev, V., and et al., (2003), Current sheet flapping motion and structure observed by Cluster, *Geophys. Res. Lett.*, 30, 1327, doi:10.1029/2002GL016500, 6.

Sergeev, V., D. A. Sormakov, S. V. Apatenkov, W. Baumjohann, R. Nakamura, A. V. Runov, T. Mukai, and T. Nagai (2006), Survey of large-amplitude flapping motions in the midtail current sheet, *Ann. Geophys.*, 24, 2015–2024.

Shen, C., Z. J. Rong, X. Li, M. Dunlop, Z. X. Liu, H. V. Malova, E. Lucek, and C. Carr (2008), Magnetic configurations of tail tilted current sheet, Ann. Geophys., 26, 3525–3543.

Slavin, J. A., et al. (2012), MESSENGER and Mariner 10 flyby observations of magnetotail structure and dynamics at Mercury, *J. Geophys. Res.*, 117, A01215, doi:10.1029/2011JA016900.

Slavin, J. A., Middleton, H. R., Raines, J. M., Jia, X., Zhong, J., Sun, W.-J., et al (2019). MESSENGER observations of disappearing dayside magnetosphere events at Mercury. *Journal of Geophysical Research: Space Physics*, 124, 6613– 6635. https://doi.org/10.1029/2019JA026892

Sonnerup, B. U., and Cahill, L. J. (1967), Magnetopause structure and attitude from Explorer 12 observations, J. Geophys. Res., 72(1), 171– 183, doi:10.1029/JZ072i001p00171.

Sonnerup, B. U. Ö., and M. Scheible(1998), Minimum and maximum variance analysis, in Analysis Methods for Multi-Spacecraft Data, edited by G. Paschmann, and P. Daly, pp. 185–220, Eur. Space Agency, Noordwijk, Netherlands.

Speiser, T. W., and Ness, N. F. (1967), The neutral sheet in the geomagnetic tail: Its motion, equivalent currents, and field line connection through it, *J. Geophys. Res.*, 72(1), 131– 141, doi:10.1029/JZ072i001p00131.

Sun, W. J., Q. Q. Shi, S.Y. Fu, Q. G. Zong, Z. Y. Pu, L. Xie, T. Xiao, L. Li, Z. X. Liu, H. Reme, E. Lucek (2010), Statistical research on the motion properties of the magnetotail current sheet: Cluster observations. *Sci China Tech Sci*, 53: 1732-1738, doi: 10.1007/s11431-010-3153-y.

Sun, W., Fu, S., Shi, Q., Zong, Q., Yao, Z., Xiao, T., & Parks, G. (2014). THEMIS observation of a magnetotail current sheet flapping wave. *Chinese science bulletin*, 59(2), 154-161.

Sun, W. J., Fu, S. Y., Slavin, J. A., Raines, J. M., Zong, Q. G., Poh, G. K., and Zurbuchen, T. H. (2016), Spatial distribution of Mercury's flux ropes and reconnection fronts: MESSENGER observations, *J. Geophys. Res. Space Physics*, 121, 7590– 7607, doi:10.1002/2016JA022787.

Sun, W. J., Fu, S. Y., Wei, Y., Yao, Z. H., Rong, Z. J., Zhou, X. Z., … Shen, X. C. (2017a). Plasma sheet pressure variations in the near-Earth magnetotail during substorm growth phase: THEMIS observations. *Journal of Geophysical Research: Space Physics*, 122, 12,212– 12,228. https://doi.org/10.1002/2017JA024603

Sun, W. J., Raines, J. M., Fu, S. Y., Slavin, J. A., Wei, Y., Poh, G. K., Pu, Z. Y., Yao, Z. H., Zong, Q. G., and Wan, W. X. (2017b), MESSENGER observations of the energization and heating of protons in the near-Mercury magnetotail, Geophys. Res. Lett., 44, 8149– 8158, doi:10.1002/2017GL074276.

Sun, W. J., Slavin, J. A., Dewey, R. M., Chen, Y., DiBraccio, G. A., Raines, J. M., et al. (2020). MESSENGER observations of Mercury's nightside magnetosphere under extreme solar wind conditions: Reconnection-generated structures and steady convection. *Journal of Geophysical Research: Space Physics*, 125, e2019JA027490. https://doi.org/10.1029/2019JA027490

Sundberg, T., Boardsen, S. A., Slavin, J. A., Anderson, B. J., Korth, H., Zurbuchen, T. H., Raines, J. M., and Solomon, S. C. (2012), MESSENGER orbital observations of large-amplitude Kelvin-Helmholtz waves at Mercury's magnetopause, *J. Geophys. Res.*, 117, A04216, doi:10.1029/2011JA017268.

Sundberg, T., et al. (2012), MESSENGER observations of dipolarization events in Mercury's magnetotail, J. Geophys. Res., 117, A00M03, doi:10.1029/2012JA017756.

Volwerk, M., et al. (2013), Comparative magnetotail flapping: An overview of selected events at Earth, Jupiter and Saturn, *Ann. Geophys.*, 31, 817–833, doi:10.5194/angeo-31-817-2013.

Wang, G. Q., Zhang, T. L., Wu, M. Y., Schmid, D., Cao, J. B., & Volwerk, M. (2019). Solar wind directional change triggering flapping motions of the current sheet: MMS observations. *Geophysical Research Letters*, 46, 64– 70. https://doi.org/10.1029/2018GL080023

Yagi, M., Seki, K., Matsumoto, Y., Delcourt, D. C., & Leblanc, F. (2017). Global structure and sodium ion dynamics in Mercury's magnetosphere with the offset dipole. *Journal of Geophysical Research: Space Physics*, 122, 10,990– 11,002. https://doi.org/10.1002/2017JA024082

Zhang, T. L., Baumjohann, W., Nakamura, R., Balogh, A., and Glassmeier, K.-H., (2002) A wavy twisted neutral sheet observed by CLUSTER, *Geophys. Res. Lett.*, 29(19), 1899, doi:10.1029/2002GL015544.

Figure 1.

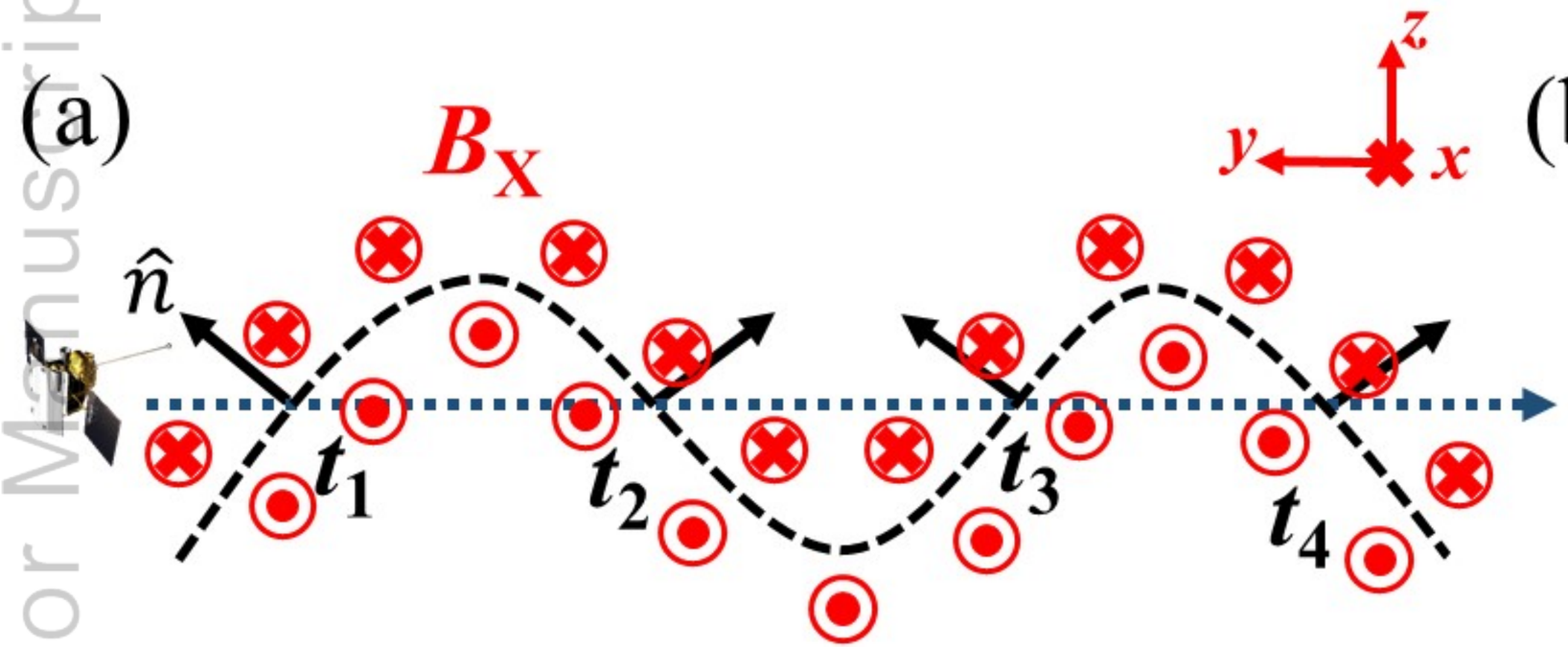

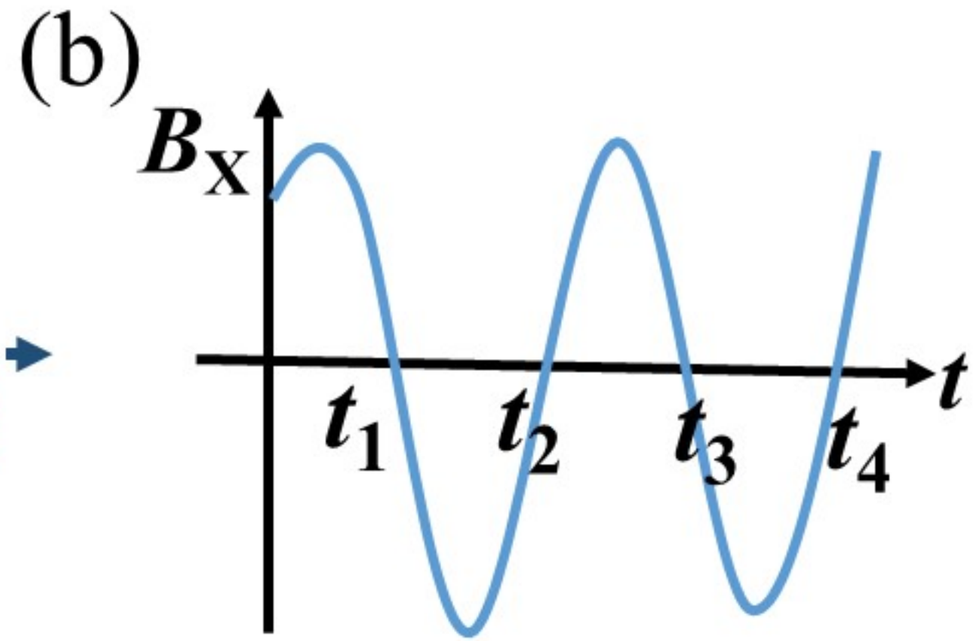

Figure 2.

(a)

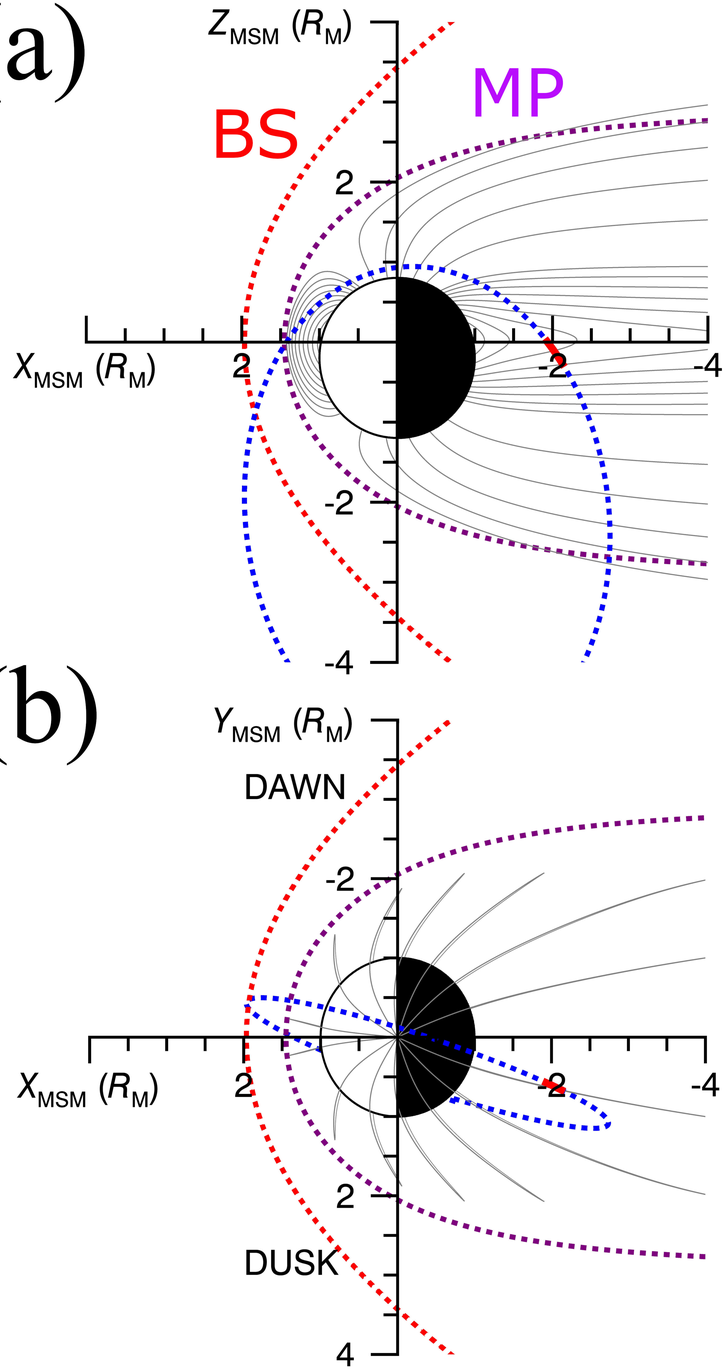

(b)

(c)

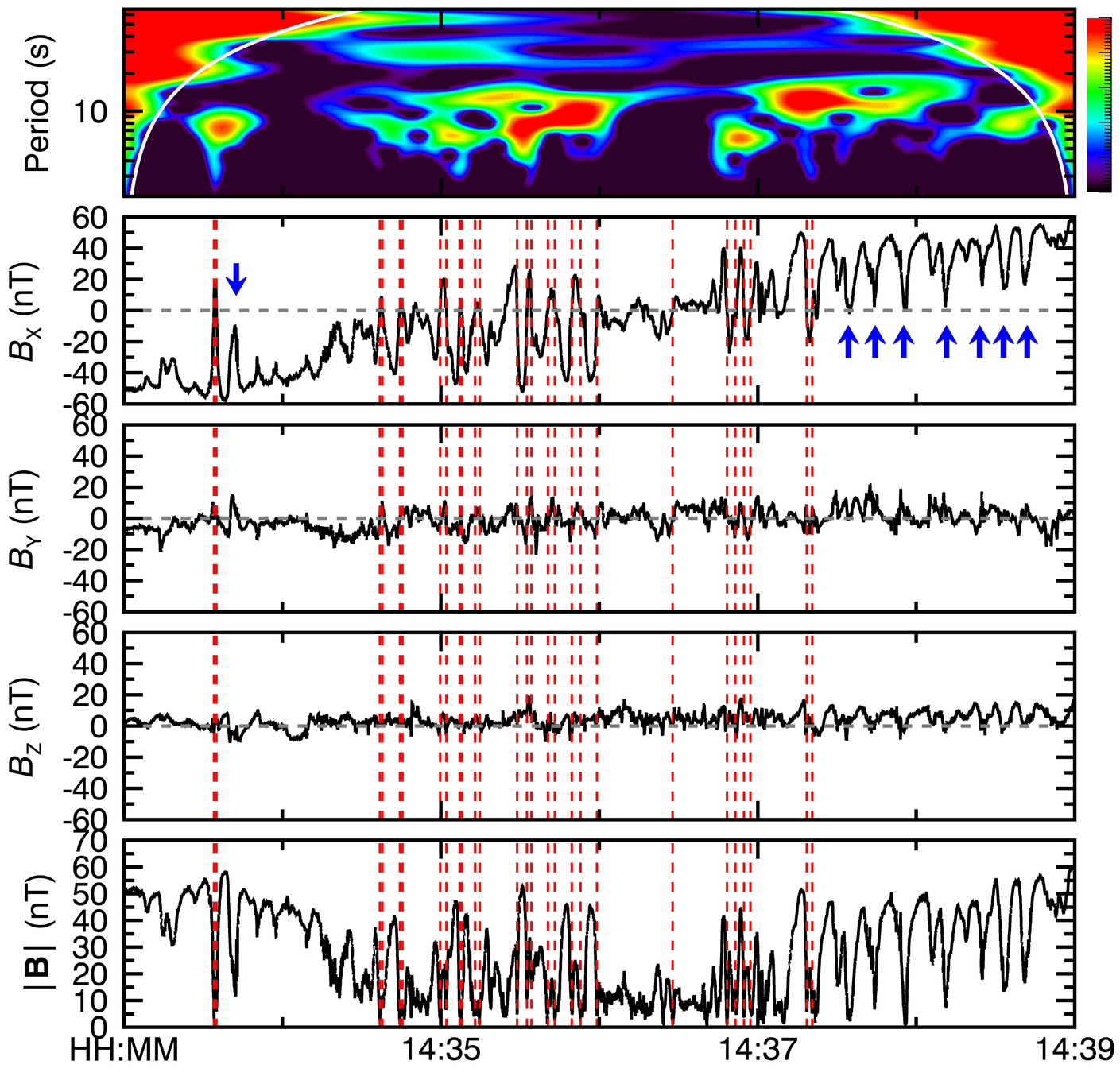

Figure 3.

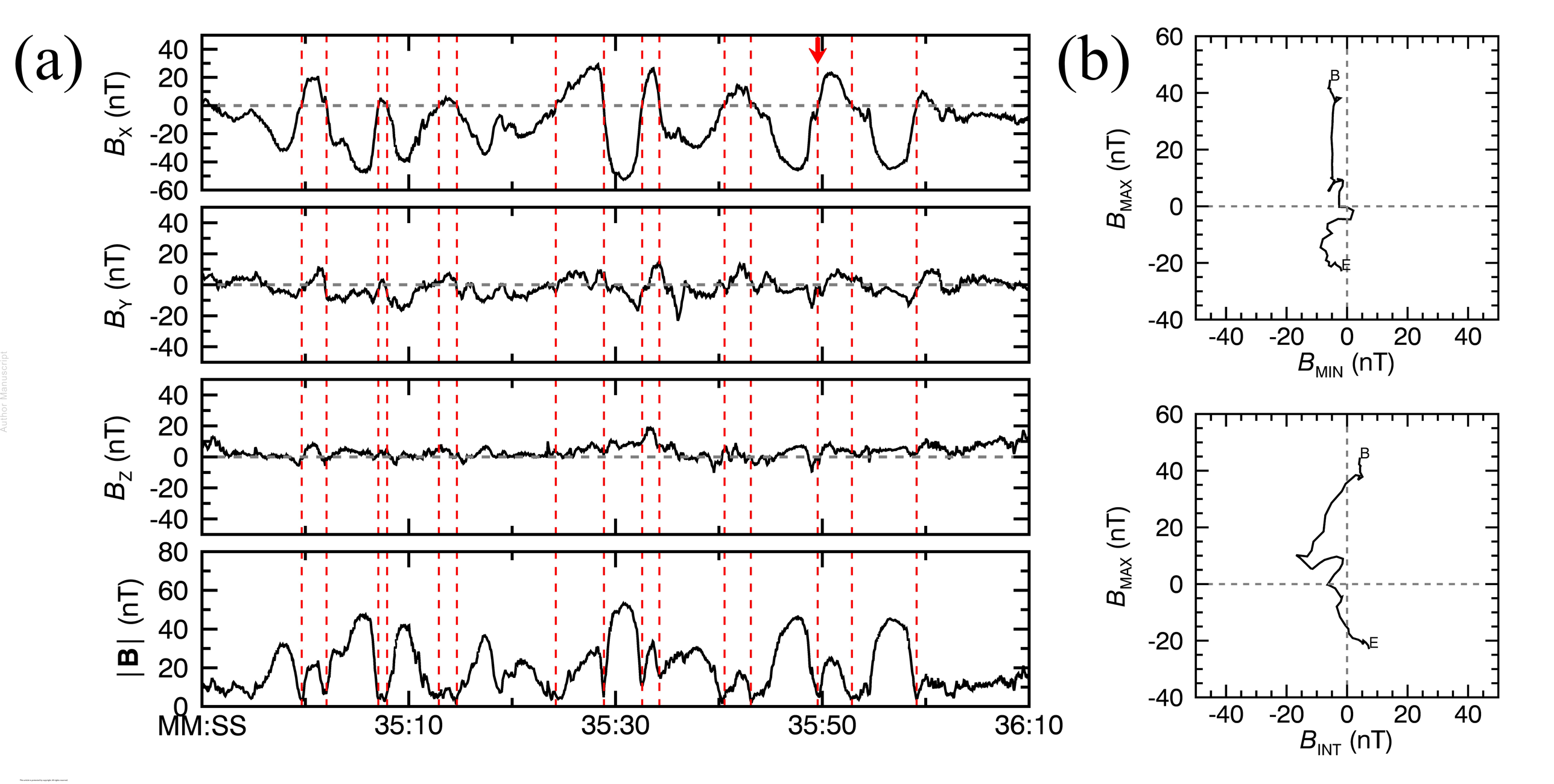

Figure 4.

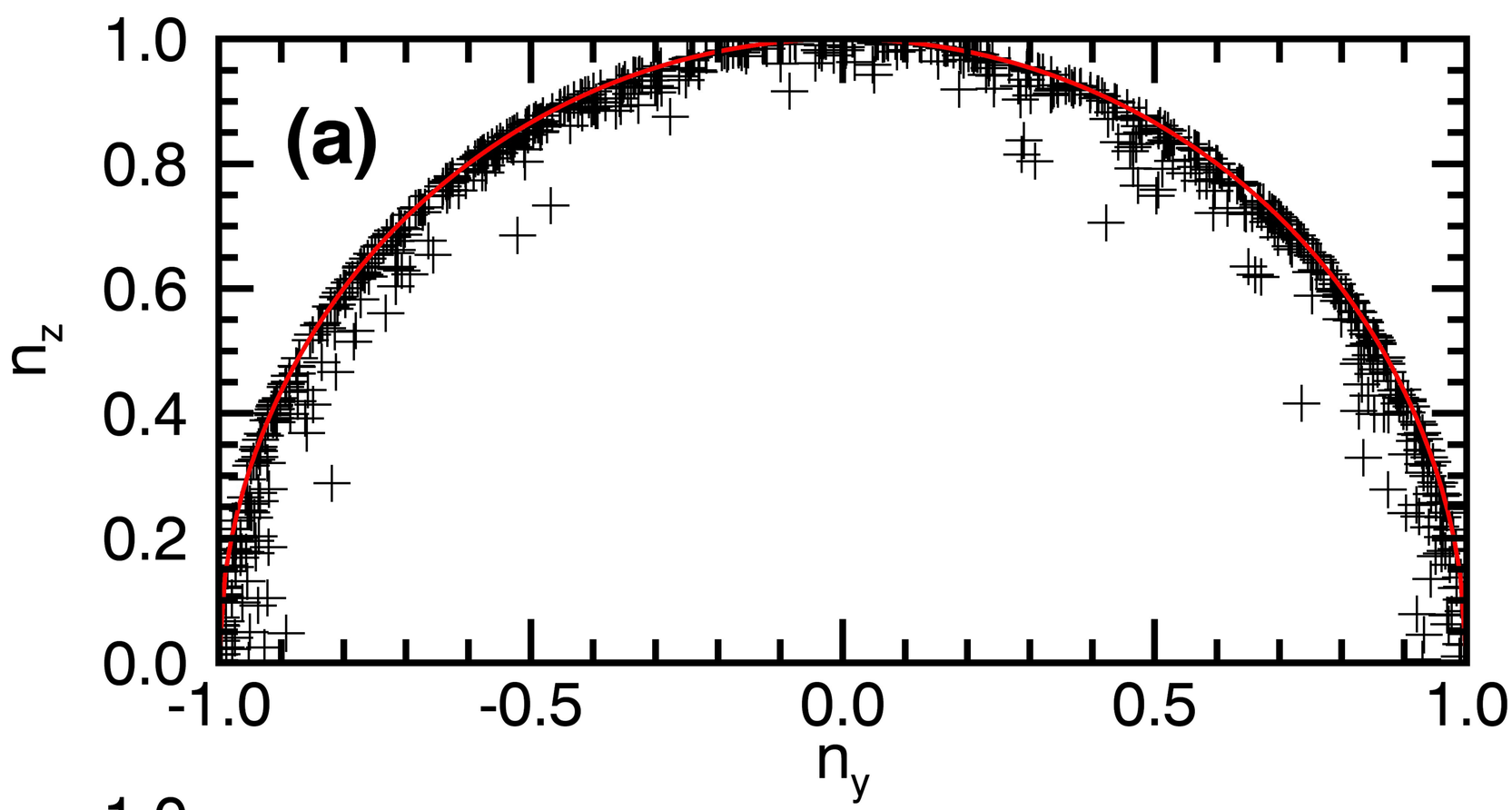

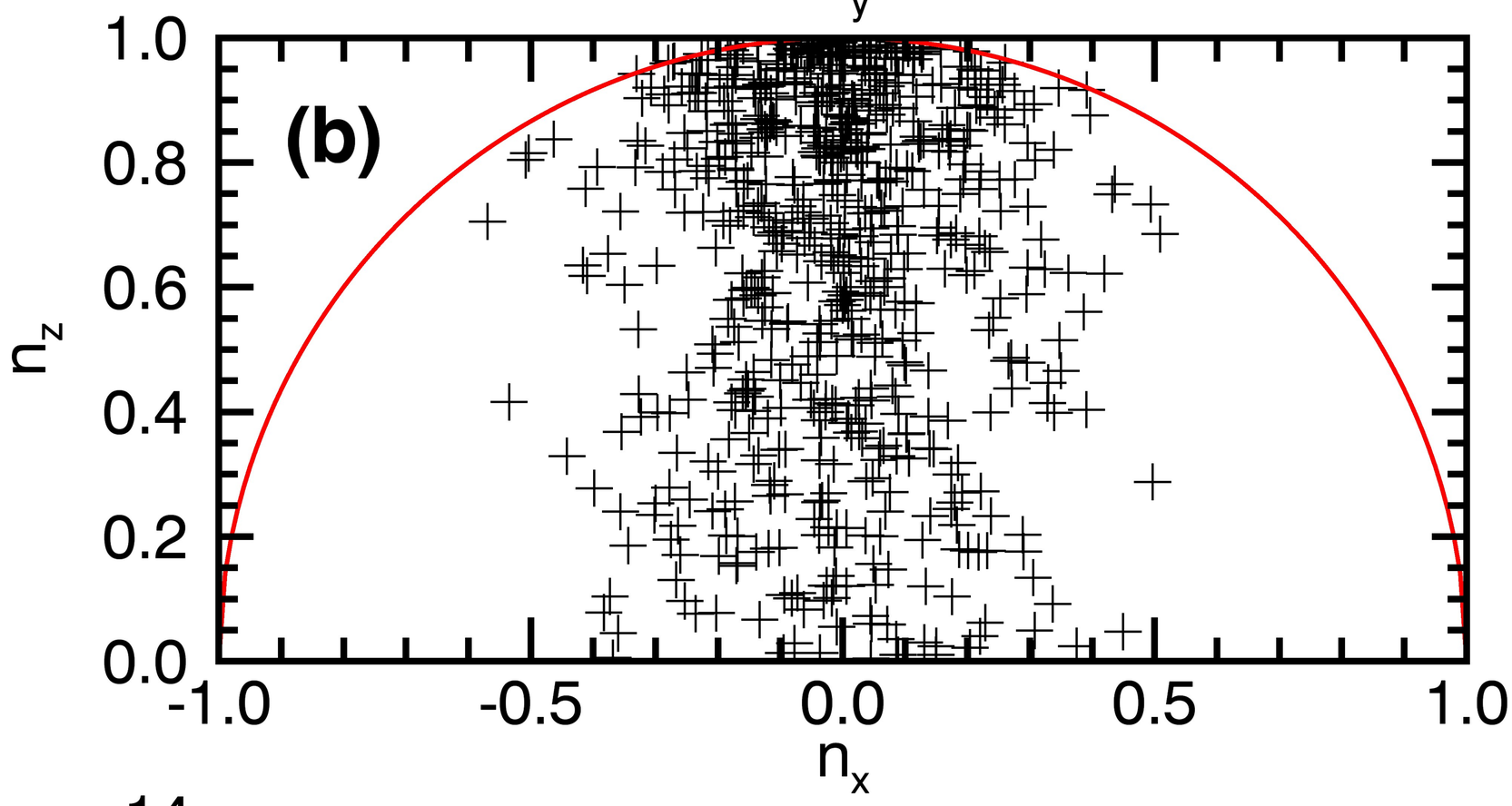

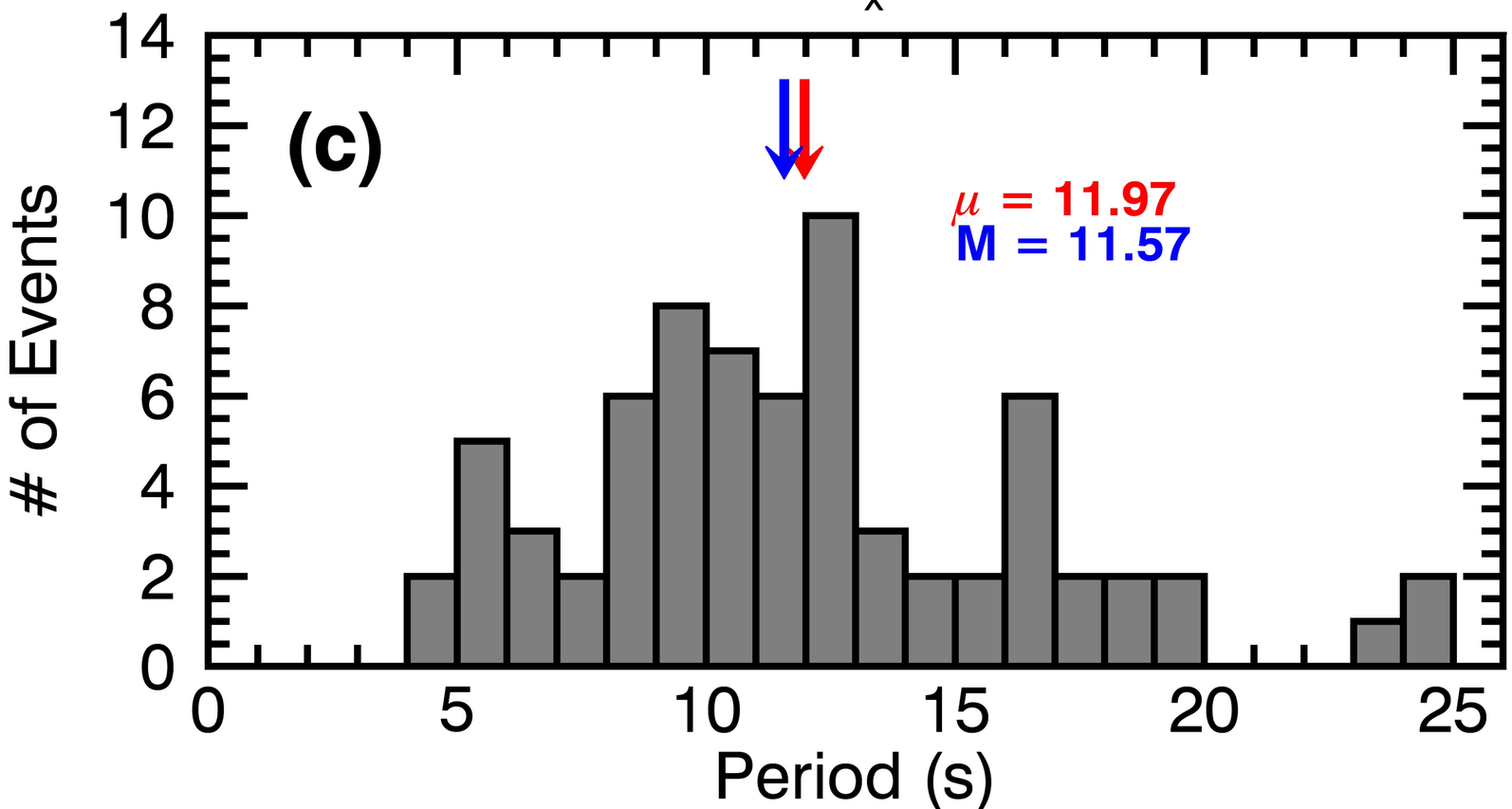

Figure 5.